Available online at www.sciencedirect.com
SCIENCE DIRECT®
Journal of Nuclear Materials 346 (2005) 272–281
journal of nuclear materials
www.elsevier.com/locate/jnucmat

Effect of self-interstitial diffusion anisotropy in electron-irradiated zirconium: A cluster dynamics modeling

F. Christien *,[1], A. Barbu

Service de Recherches de Métallurgie Physique, CEA Saclay, 91191 Gif-sur-Yvette cedex, France

Received 16 November 2004; accepted 27 June 2005

Abstract

A model based on the cluster dynamics approach was proposed in [A. Hardouin Duparc, C. Moingeon, N. Smetniansky-de-Grande, A. Barbu, J. Nucl. Mater. 302 (2002) 143] to describe point defect agglomeration in metals under irradiation. This model is restricted to materials where point defect diffusion is isotropic and is thus not applicable to anisotropic metals such as zirconium. Following the approach proposed by Woo [C.H. Woo, J. Nucl. Mater. 159 (1988) 237], we extended in this work the model to the case where self-interstitial atoms (SIA) diffusion is anisotropic. The model was then applied to the loop microstructure evolution of a zirconium thin foil irradiated with electrons in a high-voltage microscope. First, the inputs were validated by comparing the numerical results with Hellio et al. experimental results [C. Hellio, C.H. de Novion, L. Boulanger, J. Nucl. Mater. 159 (1988) 368]. Further calculations were made to evidence the effect of the thin foil orientation on the dislocation loop microstructure under irradiation. The result is that it is possible to reproduce for certain orientations the 'unexpected' *vacancy* loop growth experimentally observed in electron-irradiated zirconium [M. Griffiths, M.H. Loretto, R.E. Sallmann, J. Nucl. Mater. 115 (1983) 313; J. Nucl. Mater. 115 (1983) 323; Philos. Mag. A 49 (1984) 613]. This effect is directly linked to SIA diffusion anisotropy.

PACS: 61.72.Ji; 61.80.Fe; 61.82.Bg

1. Introduction

Zirconium alloys are used for fuel cladding in the nuclear industry and are subject to 'irradiation growth', which represents an anisotropic deformation of the material without any applied stress (see for example [7]). This irradiation growth is related to the elimination of point defects on the different sinks (dislocations lines, surfaces, grain boundaries) and also to their agglomeration in the form of dislocation loops. But in zirconium and its alloys, some aspects of dislocation loop microstructure evolution under irradiation are rather unusual compared to cubic metals, such as the growth of vacancy loops [4–6,8]. Some authors proposed that this kind of unexpected behavior could be accounted for by diffusion anisotropy of self-interstitial atoms (SIA) [2].

Concerning the modeling of the loop microstructure evolution under irradiation, a model based on the cluster dynamics approach was proposed in [1]. Nevertheless, as

* Corresponding author. Tel.: +33 2 40 68 3161; fax: +33 2 40 68 3199.
E-mail address: frederic.christien@polytech.univ-nantes.fr (F. Christien).
[1] Present address: LGMPA, Polytech Nantes, BP 50609, Nantes cedex 3, France.

0022-3115/$ - see front matter © 2005 Elsevier B.V. All rights reserved.
doi:10.1016/j.jnucmat.2005.06.024

far as zirconium is concerned, this model is not applicable because it is based on the assumption that point defects diffuse isotropically, which is not true for zirconium. Indeed, diffusion of point defects in zirconium is known to be anisotropic, specially for SIA [9–11].

This papers aims at extending the cluster model presented in [1] to the case where point defect diffusion is anisotropic, using the approach proposed by Woo [2]. After reminding the reader of the main equations of the cluster model, we will show how it is possible to extend the model to anisotropic diffusion. It will then be applied to describe the evolution of the dislocation loop microstructure in an electron-irradiated zirconium thin foil.

2. The cluster dynamics model

Equations: We will first set the basic equations of the model for a medium where point defect diffusion is supposed to be isotropic [1]. The evolution of the loop size distribution under electron irradiation is obtained by resolving the following differential equations system:

$$\begin{aligned}
\frac{dC_{ni}}{dt} &= [\beta^i_{(n-1)i}C_{1i}]C_{(n-1)i} + [\beta^v_{(n+1)i}C_{1v} + \alpha^i_{(n+1)i}]C_{(n+1)i} \\
&\quad - [\alpha^i_{ni} + \beta^v_{ni}C_{1v} + \beta^i_{ni}C_{1i}]C_{ni}, \\
\frac{dC_{nv}}{dt} &= [\beta^v_{(n-1)v}C_{1v}]C_{(n-1)v} + [\beta^i_{(n+1)v}C_{1i} + \alpha^v_{(n+1)v}]C_{(n+1)v} \\
&\quad - [\alpha^v_{nv} + \beta^i_{nv}C_{1i} + \beta^v_{nv}C_{1v}]C_{nv}, \\
\frac{dC_{1i}}{dt} &= G - R_{iv}C_{1i}C_{1v} - K^i_dC_{1i} - K^i_sC_{1i} \\
&\quad - 2\beta^i_{1i}C_{1i}C_{1i} + 2\alpha^i_{2i}C_{2i} + \beta^v_{2i}C_{1v}C_{2i} \\
&\quad - C_{1i}\sum_{n=2}^{\infty}\beta^i_{ni}C_{ni} - C_{1i}\sum_{n=2}^{\infty}\beta^i_{nv}C_{nv} + \sum_{n=3}^{\infty}\alpha^i_{ni}C_{ni}, \qquad (1) \\
\frac{dC_{1v}}{dt} &= G - R_{iv}C_{1i}C_{1v} - K^v_dC_{1v} - K^v_sC_{1v} \\
&\quad - 2\beta^v_{1v}C_{1v}C_{1v} + 2\alpha^v_{2v}C_{2v} + \beta^i_{2v}C_{1i}C_{2v} - C_{1v}\sum_{n=2}^{\infty}\beta^v_{nv}C_{nv} \\
&\quad - C_{1v}\sum_{n=2}^{\infty}\beta^v_{ni}C_{ni} + \sum_{n=3}^{\infty}\alpha^v_{nv}C_{nv}, \\
\frac{dC_{2i}}{dt} &= \beta^i_{1i}C_{1i}C_{1i} - \alpha^i_{2i}C_{2i} - \beta^i_{2i}C_{1i}C_{2i} \\
&\quad + \alpha^i_{3i}C_{3i} - \beta^v_{2i}C_{1v}C_{2i} + \beta^v_{3i}C_{1v}C_{3i}, \\
\frac{dC_{2v}}{dt} &= \beta^v_{1v}C_{1v}C_{1v} - \alpha^v_{2v}C_{2v} - \beta^v_{2v}C_{1v}C_{2v} \\
&\quad + \alpha^v_{3v}C_{3v} - \beta^i_{2v}C_{1i}C_{2v} + \beta^i_{3v}C_{1i}C_{3v}.
\end{aligned}$$

n is the number of monomers (vacancies or SIA) included in a cluster (loop) of size n, $C_{n\theta}$ is the concentration of the clusters of size n per unit volume (with $\theta = i$ for interstitials (SIA) and $\theta = v$ for vacancies), $\beta^{\theta'}_{n\theta}C_{1\theta'}$ is the frequency at which a cluster of type θ absorbs a defect of type θ', $\alpha^{\theta}_{n\theta}$ is the frequency at which a cluster of type θ emits a defect of type θ, R_{iv} is the vacancy-SIA recombination rate, $K^{\theta}_dC_{1\theta}$ is the absorption rate of the defects of type θ by the dislocation lines, $K^{\theta}_sC_{1\theta}$ is the absorption rate of the defects of type θ by the surfaces. G is the point defect creation rate, i.e. the number of Frenkel pairs (1 Frenkel pair = 1 vacancy + 1 SIA) created under electron irradiation per second and per cm^3. G is also often expressed in dpa s^{-1} (dpa = displacement per atom). The differential equation system (1) is based on the assumptions that only monomers (vacancies and SIA) are mobile and that a cluster of type θ can emit point defects of the same type only. It can be shown that the latter assumption is realistic provided that the point defect supersaturation is large, which will be the case here since the point defect production rate is high ($G = 1.5 \times 10^{-4}$ dpa s^{-1}, see Table 1).

Rate coefficients: The expressions of the rate coefficients appearing in the differential equations system (1) are presented below.

2.1. SIA-vacancy recombination

The recombination rate R_{iv} is given by

$$R_{iv} = 4\pi r_{iv}(D_i + D_v). \qquad (2)$$

r_{iv} is the recombination radius, D_i and D_v are the SIA and vacancy diffusion coefficients respectively.

2.2. Absorption of point defects by dislocation lines

The absorption rate $K^{\theta}_dC_{1\theta}$ of the defects of type θ by the dislocation lines is

$$K^{\theta}_dC_{1\theta} = \rho Z^{\theta}_dD_{\theta}C_{1\theta}. \qquad (3)$$

ρ is the dislocation density in the material, D_θ is the diffusion coefficient of the defect of type θ and Z^{θ}_d is a dimensionless factor which represents the absorption efficiency of point defects by the dislocation lines. This factor makes it possible to take the elastic interaction between point defects and dislocations into account. Z^{θ}_d is usually taken equal to 1 for vacancies (no elastic interaction) and about 1.1–1.2 for SIA.

2.3. Absorption of point defects by dislocation loops

The absorption frequency $\beta^{\theta'}_{n\theta}C_{1\theta'}$ of a defect of type θ' by a loop of type θ is

$$\beta^{\theta'}_{n\theta}C_{1\theta'} = 2\pi r_nZ^{\theta'}_{n\theta}D_{\theta'}C_{1\theta'}. \qquad (4)$$

r_n is the cluster radius. If we make the assumption that the point defects agglomerate to form dislocation loops, r_n can be written as follows:

$$r_n = \sqrt{\frac{nV_{at}}{\pi b}}. \qquad (5)$$

Table 1
Parameters introduced into the model to describe the evolution of the dislocation loop microstructure in an electron-irradiated Zr thin foil

	Symbol	Value	Refs.
Point defect creation rate	G	1.5×10^{-4} dpa s^{-1}	[3]
Foil thickness	$2d$	0.5×10^{-4} cm	[3]
Dislocation line density	ρ	10^{8} cm^{-2}	Annealed
SIA formation energy	E_i^{f}	3.77 eV	[17]
Vacancy formation energy	E_v^{f}	1.79 eV	[17]
Di-interstitial binding energy	E_{2i}^{B}	1.42 eV	Adjusted
Di-vacancy binding energy	E_{2v}^{B}	0.22 eV	[18]
SIA diffusion coefficient			
Along the a-axis	D_i^a	$3.5\times10^{-4}\exp\left(-\frac{0.06\,\mathrm{eV}}{kT}\right)$ cm^2 s^{-1}	[11]
Along the c-axis	D_i^c	$4.7\times10^{-4}\exp\left(-\frac{0.15\,\mathrm{eV}}{kT}\right)$ cm^2 s^{-1}	[11]
Vacancy diffusion coefficient	D_v	$2.2\times10^{-2}\exp\left(-\frac{0.93\,\mathrm{eV}}{kT}\right)$ cm^2 s^{-1}	[11]
Recombination radius	r_{iv}	10^{-7} cm	[19]
SIA/dislocation elastic interaction	$Z_{d\,\mathrm{iso}}^{i}$	1.1	[2,20]
Vacancy/dislocation elastic interaction	Z_d^v	1.0	
Bürgers vector (prismatic loops)	b	3.23×10^{-8} cm	[8]

V_{at} is the atomic volume and b is the Bürgers vector of the dislocation loop. In Eq. (4) $Z_{n\theta}^{\theta'}$ is an efficiency factor that makes it possible to take the defect-dislocation elastic interaction and also the toroidal shape of the loop into account; $Z_{n\theta}^{\theta'}$ depends on the loop size:

$$Z_{n\theta}^{\theta'} = Z_d^{\theta}\max\left\{\frac{2\pi}{\ln\left(\frac{8r_n}{r_{\mathrm{p}}}\right)},1\right\}. \tag{6}$$

r_{p} is the pipe radius of the dislocation and is usually taken equal to $2b$. Eq. (6) is a simplified expression of Eq. (14) in [1].

2.4. Absorption of point defects by surfaces

The absorption rate $K_{\mathrm{s}}^{\theta}C_{1\theta}$ of the defects of type θ by two parallel surfaces separated by a distance $2d$ is given by [12]:

$$K_{\mathrm{s}}^{\theta}C_{1\theta} = \frac{\sqrt{S_m^{\theta}}}{d}\frac{D_{\theta}C_{1\theta}}{\coth\left(\sqrt{S_m^{\theta}}d\right)-\frac{1}{\sqrt{S_m^{\theta}}d}}, \tag{7}$$

where S_m^{θ} represents the total sink strength of the medium without the surfaces (dislocation lines + dislocation loops):

$$S_m^{\theta} = \rho Z_d^{\theta} + \frac{1}{D_{\theta}}\sum_{n=2}^{\infty}\left(\beta_{n\theta}^{\theta}C_{n\theta}+\beta_{n\theta'}^{\theta}C_{n\theta'}\right). \tag{8}$$

According to the value of $\sqrt{S_m^{\theta}}d$, Eq. (7) can be simplified. If $\sqrt{S_m^{\theta}}d \ll 1$, Eq. (7) reduces to:

$$K_{\mathrm{s}}^{\theta}C_{1\theta} = \frac{3}{d^2}D_{\theta}C_{1\theta}. \tag{9}$$

Eq. (9) corresponds to the situation where absorption on the surfaces is much greater than absorption in the bulk (on dislocation lines and loops). On the contrary, if $\sqrt{S_m^{\theta}}d \gg 1$, Eq. (7) reduces to:

$$K_{\mathrm{s}}^{\theta}C_{1\theta} = \frac{\sqrt{S_m^{\theta}}}{d}D_{\theta}C_{1\theta}. \tag{10}$$

Eq. (10) corresponds to the situation where absorption in the bulk (on dislocation lines and loops) is much greater than absorption on the surfaces.

2.5. Emission of point defects by dislocation loops

It is assumed that point defects of type θ can be emitted only by loops of the same type at a frequency $\alpha_{n\theta}^{\theta}$ that is given by

$$\alpha_{n\theta}^{\theta} = 2\pi r_{n-1}Z_{(n-1)\theta}^{\theta}D_{\theta}\frac{\exp\left(-E_{n\theta}^{\mathrm{B}}/kT\right)}{V_{\mathrm{at}}}, \tag{11}$$

where $E_{n\theta}^{\mathrm{B}}$ is the binding energy of a defect of type θ to a loop of the same type:

$$E_{n\theta}^{\mathrm{B}} = E_{\theta}^{\mathrm{f}} - \left(E_{n\theta}^{\mathrm{f}} - E_{(n-1)\theta}^{\mathrm{f}}.\right) \tag{12}$$

E_{θ}^{f}, $E_{n\theta}^{\mathrm{f}}$ and $E_{(n-1)\theta}^{\mathrm{f}}$ represent the formation energies of the point defect, of a loop containing n defects and of a loop containing $n-1$ defects respectively. It is usually possible to evaluate $E_{n\theta}^{\mathrm{B}}$ as a function of n through an analytical expression. In this work, we will use the following equation [1,13]:

$$E^{B}_{n\theta} = E^{f}_{\theta} + \frac{E^{B}_{2\theta} - E^{f}_{\theta}}{2^{2/3} - 1}\left(n^{2/3} - (n-1)^{2/3}\right). \quad (13)$$

$E^{B}_{2\theta}$ is the binding energy of the dimer (di-interstitial or di-vacancy).

2.6. Comment about the binding energy

The definition of the binding energy we choose here is given in Eq. (12). It is found sometimes another definition which is

$$\epsilon^{B}_{n\theta} = \frac{nE^{f}_{\theta} - E^{f}_{n\theta}}{n}. \quad (14)$$

These two binding energies $E^{B}_{n\theta}$ and $\epsilon^{B}_{n\theta}$ are of course not independent: if one knows $E^{B}_{n\theta}$ for every n, it is possible to calculate $\epsilon^{B}_{n\theta}$ for every n thanks to the following recurrent relation:

$$\begin{cases} \epsilon^{B}_{1\theta} = 0, \\ \epsilon^{B}_{n\theta} = nE^{B}_{n\theta} - (n-1)\epsilon^{B}_{(n-1)\theta}. \end{cases} \quad (15)$$

Outputs of the model: By solving the differential equations system (1), one gets the evolution with time of the vacancy and interstitial loop size distributions. From these distributions, it is possible to calculate measurable values such as the *loop mean radius* or the *total loop density*. It is also possible to calculate the *loop growth speed*. For example, if we assume that only interstitial loops form, the loop growth speed is given by [14]:

$$\dot{r_n} = \frac{V_{at}}{b}\left(Z^{i}_{ni}D_iC_{1i} - Z^{v}_{ni}D_vC_{1v}\right). \quad (16)$$

Eq. (16) can easily be derived using Eq. (4) and Eq. (5). For sufficiently large loops, the efficiency factors Z^{i}_{ni} and Z^{v}_{ni} do not depend on the loop radius (see Eq. (6)). Moreover, when the steady state is reached, the SIA and vacancy concentrations C_{1i} and C_{1v} are constant. That is why, for large loops and when the steady state is reached, the loop growth speed $\dot{r_n}$ can be considered constant.

3. Extension of the cluster dynamics model to anisotropic diffusion

The dislocation loops that form in zirconium during electron or neutron irradiation can be classified in two main groups according to the orientation of their Bürgers vector:

- The *a* loops or *prismatic* loops: they lie approximately in the prismatic planes $\{10\bar{1}0\}$ and have a Bürgers vector $b = 1/3[11\bar{2}0]$. Both vacancy and interstitial loops can be observed simultaneously under neutron or electron irradiation [4–6,8].
- The *c* loops or *basal* loops: they lie in the basal planes $\{0001\}$ and their Bürgers vector has a component along the *c*-axis. These loops can be perfect ($b = [0001]$) or unperfect ($b = 1/6[20\bar{2}3]$ and $b = 1/2[0001]$).

During irradiation, prismatic loops form first. Nucleation and growth of c-component loops are observed only above a certain irradiation dose that depends on the alloying elements and the temperature [8,15]. We consider here a thin foil irradiated with electrons in a high voltage microscope and make the assumption that the irradiation dose is low enough so that *c* loops do not form. That is why only the prismatic loops will be taken into account here. The point defect sinks that will be considered in the material are listed below:

- the *a* loops,
- the dislocation lines present before irradiation,
- the thin foil surfaces.

Following the approach proposed by Woo [2], the rate coefficients of the cluster model can be modified in order to take the SIA diffusion anisotropy into account in the cluster dynamics model. Vacancy diffusion will be considered isotropic [11]. We define the SIA diffusion anisotropy factor p and the mean diffusion coefficient $\bar{D}_i$:

$$p = \left(\frac{D^{c}_{i}}{D^{a}_{i}}\right)^{1/6}, \quad (17)$$

$$\bar{D}_i = \left(D^{a2}_{i}D^{c}_{i}\right)^{1/3}, \quad (18)$$

where D^{a}_{i} is the SIA diffusion coefficient in the basal plane (i.e. along the *a*-axis) and D^{c}_{i} is the SIA diffusion coefficient along the *c*-axis. In zirconium, $D^{a}_{i} > D^{c}_{i}$ so that $p < 1$ [9–11].

3.1. SIA-vacancy recombination

The recombination rate R_{iv} is simply:

$$R_{iv} = 4\pi r_{iv}(\bar{D}_i + D_v). \quad (19)$$

3.2. Absorption of SIA by dislocation lines

Let us consider a dislocation line making an angle λ with the *c*-axis. The anisotropic diffusion effect can be taken into account in the efficiency factor Z^{i}_{d} (see Eq. (3)):

$$Z^{i}_{d} = Z^{i}_{d_{iso}} \times P(\lambda). \quad (20)$$

$Z^{i}_{d_{iso}}$ is the efficiency factor for isotropic diffusion that simply represents the elastic interaction defect-dislocation. $P(\lambda)$ is given by

$$P(\lambda) = \frac{\sqrt{\cos^2\lambda + p^6\sin^2\lambda}}{p^2}. \quad (21)$$

We will make here the assumption that all the dislocation lines are parallel to the c-axis (this assumption has in fact very little effect since the dislocation density is low). Then $\lambda = 0$ and the absorption rate $K_d^i C_{1i}$ of the SIA by the dislocation lines is

$$K_d^i C_{1i} = \frac{\rho Z_{d\mathrm{iso}}^i}{p^2} \bar{D}_i C_{1i}. \tag{22}$$

3.3. Absorption of SIA by dislocation loops

The calculation of the efficiency factor $Z_{n\theta}^i$ for the absorption of SIA by a prismatic dislocation loop is not as simple as for a straight dislocation. Indeed, for a prismatic loop, the angle between the dislocation line and the c-axis is not constant. That is why we propose to represent a loop by an hexagon with the same perimeter (Fig. 1). We choose to orientate the hexagon so that two sides are perpendicular to the c-axis. Each side of the hexagon has a length h and is characterized by an efficiency factor $Z_j, j = 1, \ldots, 6$ that depends on its orientation with respect to the c-axis. The absorption frequency $\beta_{n\theta}^i C_{1i}$ of SIA by a loop of size n is

$$\beta_{n\theta}^i C_{1i} = 2\pi r_n Z_{n\theta}^i \bar{D}_i C_{1i} = \left(\sum_{j=1}^{6} h Z_j \right) \bar{D}_i C_{1i} \tag{23}$$

with

$$Z_1 = Z_4 = Z_{n\theta\mathrm{iso}}^i \times P(\pi/2) = Z_{n\theta\mathrm{iso}}^i \times p \tag{24}$$

and

$$Z_2 = Z_3 = Z_5 = Z_6 = Z_{n\theta\mathrm{iso}}^i \times P(\pi/6) = Z_{n\theta\mathrm{iso}}^i \times \frac{\sqrt{3+p^6}}{2p^2}. \tag{25}$$

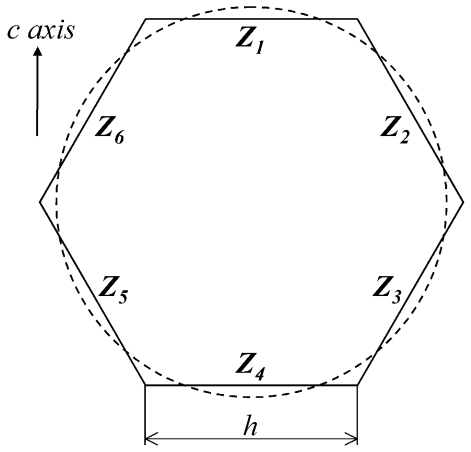

Fig. 1. Representation of the loop by an hexagon with the same perimeter.

$Z_{n\theta\mathrm{iso}}^i$ is the efficiency factor relative to the absorption of SIA by dislocation loops when SIA diffusion is assumed isotropic. $Z_{n\theta\mathrm{iso}}^i$ is given by Eq. (6). Taking into account that $2\pi r_n = 6h$ and introducing the expressions of Z_j into Eq. (23), we get:

$$Z_{n\theta}^i = Z_{n\theta\mathrm{iso}}^i \times Z_a^i, \tag{26}$$

where Z_a^i is a parameter depending on the SIA diffusion anisotropy:

$$Z_a^i = \frac{1}{3}\left(p + \frac{\sqrt{3+p^6}}{p^2} \right). \tag{27}$$

3.4. Absorption of SIA by surfaces

The absorption rate $K_s^i C_{1i}$ of the SIA by two parallel surfaces separated by a distance $2d$ can be calculated by Eq. (7) provided that d is replaced by d':

$$d' = d \times \frac{p}{\sqrt{\sin^2\lambda + p^6 \cos^2\lambda}}, \tag{28}$$

where λ is the angle between the c-axis and the normal to the surfaces.

3.5. Emission of SIA by dislocation loops

Eq. (11) remains valid when diffusion is anisotropic. The term $Z_{(n-1)i}^i$ appearing in Eq. (11) is calculated using Eq. (26).

4. Application of the model to electron irradiated zirconium

4.1. Validation of the inputs

The cluster dynamics model presented above was applied to describe the evolution of the dislocation loop microstructure in a pure zirconium thin foil irradiated with electrons in a high voltage microscope. In order to validate the input parameters, the results of the model were first compared to the experimental results of Hellio et al. [3]. In that study, the authors have irradiated in a high voltage (1 MeV) electron microscope good purity zirconium (Van Arkel zirconium containing 50 ppm oxygen) and zirconium containing 1760 ppm oxygen. The defect creation rate is 1.5×10^{-4} dpa s^{-1}, the foil thickness is about 0.5 μm and the angle between the normal to the surfaces and the c-axis is $\lambda = 30°$. The nature of the dislocation loops observed in Zr-1760 ppm O was analyzed: the loops were found to be of interstitial type. Although the authors did not experimentally analyze the nature of the loops observed in pure zirconium, they made the assumption that the loops were also of interstitial type in pure zirconium as directly checked for

Zr-1760 ppm O (see Section 4.1 of [3]). Following the authors Hellio et al., it seems reasonable to assume that the loops observed in pure zirconium in [3] are interstitial in nature. These loops lie approximately in the prismatic planes. The authors have measured the evolution of the loop density with irradiation time and also the loop growth speed at several temperatures. They observed that irradiation times of a few hundreds of seconds are sufficient to reach a steady state loop density (Fig. 3).

We tried in this study to reproduce by the cluster dynamics model the steady state loop density and loop growth speed. The parameters introduced in the model are listed in Table 1. All the physical parameters relative to zirconium were taken from the literature, except E_{2i}^{B} the binding energy of the di-interstitial, that was used as a fitting parameter. This parameter E_{2i}^{B} is needed in the model to calculate the binding energy of the interstitial loops as a function of their size thanks to Eq. (13). The comparison between experimental results and calculation by the model is presented in Fig. 2 and shows a good agreement. The fitting procedure leads to $E_{2i}^{B} = 1.42$ eV. Taking this value of E_{2i}^{B} and using Eq. (13) and Eq. (15), it is possible to calculate the binding energy ϵ_{ni}^{B} as a function of n, the number of SIA included in a loop. ϵ_{ni}^{B} is shown in Fig. 4. A good agreement is found with values obtained by de Diego et al. [16] for several n using molecular dynamics simulations based on the Ackland potential [17].

4.2. Influence of the foil orientation

In the study by Hellio et al. [3], the crystallographic orientation of the thin foil was always the same: the angle between the normal to the surfaces and the c-axis was $\lambda = 30°$. In that case, only interstitial loops are observed and the loop microstructure is not very sensitive to the SIA diffusion anisotropy: indeed the results of the cluster dynamics model shown on Fig. 2 are quite similar if we impose that the SIA anisotropy factor p defined by Eq. (17) is equal to 1.0. Nevertheless, it can be expected that for other foil orientations, the SIA diffusion anisotropy could influence the loop microstructure. Indeed, the

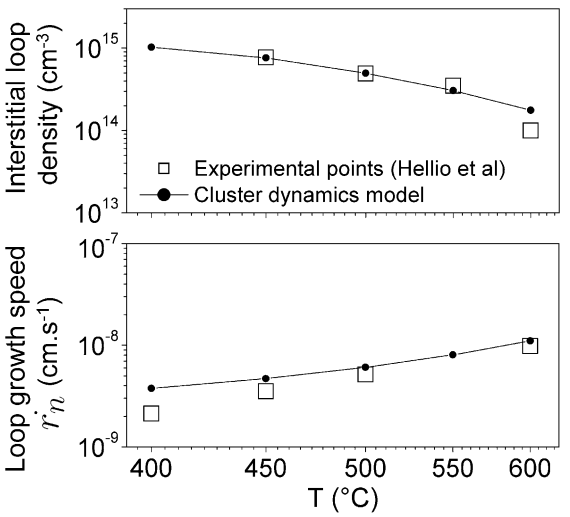

Fig. 2. Steady state interstitial loop density and loop growth speed. Experimental results of Hellio et al. [3] on pure Zr and calculation by the cluster dynamics model. The parameters that were introduced in the model are listed in Table 1.

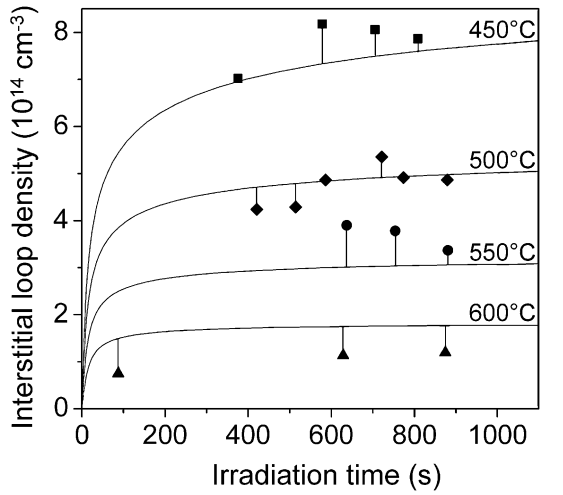

Fig. 3. Evolution with time of the interstitial loop density. Experimental results of Hellio et al. [3] on pure Zr and calculation by the cluster dynamics model. The parameters that were introduced in the model are listed in Table 1.

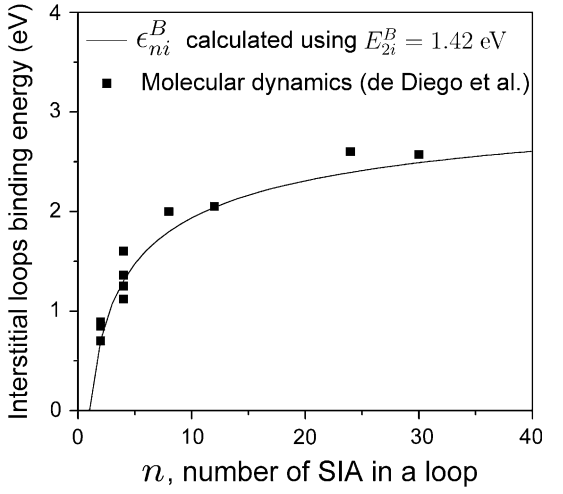

Fig. 4. Interstitial loops binding energy. The line corresponds to the calculation of ϵ_{ni}^{B} using Eq. (13) and Eq. (15) with $E_{2i}^{B} = 1.42$ eV. It is in good agreement with the values of de Diego et al. [16] obtained by molecular dynamics simulations using the Ackland potential [17].

absorption rate of the SIA by the foil surfaces strongly depends on the foil orientation (Eqs. (7) and (28)). That is why it seemed interesting to us to study thanks to the cluster dynamics model the influence of the foil orientation (i.e. the angle λ between the normal to the foil surfaces and the c crystallographic axis) on the loop microstructure. We choose a temperature of 300 °C. The inputs parameters of the model are listed in Table 1. The irradiation time is chosen so as to reach an irradiation dose of 10 dpa. Fig. 5 shows the interstitial and vacancy loop size distributions obtained in three different situations: in Fig. 5(a), the SIA diffusion is supposed isotropic (i.e. the parameter p defined in Eq. (17) is taken equal to one in the model); in Fig. 5(b), the SIA diffusion anisotropy is taken into account ($p = 0.775$ at 300 °C) and the c-axis is taken normal to the foil surfaces ($\lambda = 0$); in Fig. 5(c), the SIA diffusion anisotropy is also taken into account ($p = 0.775$) and the c-axis is taken parallel to the foil surfaces ($\lambda = 90°$). The result obtained in case (a) is very classical since we observe interstitial loop growth, which can be attributed to the preferential absorption of SIA on dislocation loops due to the SIA-dislocation elastic interaction [1]. It can be observed that in case (b), interstitial loop growth is slightly favored compared to case (a). On the contrary, interstitial loop growth is strongly disfavored in case (c) since we observed *vacancy* loop growth.

The same kind of calculation was made again for several different foil orientations. From the loop size distributions that were obtained, we calculated the total loop density and the loop mean radius. The total loop density and the loop mean radius are plotted in Fig. 6 as a function of the angle λ. The full circles correspond to interstitial loops and the empty circles to vacancy loops. In Fig. 6(a1) and (a2), the SIA diffusion anisotropy is supposed isotropic ($p = 1$) whereas in Fig. 6(b1) and (b2) the SIA diffusion anisotropy is taken into account.

The calculations presented in Figs. 5 and 6 show that for small λ angles, SIA diffusion anisotropy leads to interstitial loop densities and interstitial loop radius slightly higher than when the diffusion is assumed isotropic. In other words, when λ is small, SIA diffusion anisotropy make the interstitial loops nucleation and growth easier. This can be interpreted as follows: when λ is small, the basal planes are rather parallel to the foil surfaces; as a consequence, SIA move rather parallel to the foil surfaces since $D_i^a > D_i^c$. The probability that a SIA is absorbed by the surfaces is then reduced. That is why SIA agglomerate to form loops, rather than eliminate on the foil surfaces.

On the contrary, when λ is high, the basal planes are rather perpendicular to the foil surfaces; SIA move rather perpendicularly to the foil surfaces, which increases the absorption rate of SIA by the surfaces. It follows that the loops absorb less SIA, so that the growth of vacancy loops can become possible.

It is interesting to note that the situation described on Fig. 6 is very binary: below $\lambda_0 \approx 60°$, the behavior is rather 'classical' (growth of interstitial loops); on the contrary, above $\lambda_0 \approx 60°$, the situation is characterized by a 'non-classical' growth of vacancy loops. In order to understand why the situation is changed at about $\lambda_0 \approx 60°$, the concept of 'bias' [2] will be very useful here. The bias associated with a kind of sink enables us to predict whether the considered sink will absorb more SIA or more vacancies. We have here two main kinds of sinks: the prismatic dislocation loops and the foil surfaces (the absorption of point defects on dislocation lines can be neglected here). The biases B_l and B_s of prismatic loops and foil surfaces respectively are defined as follows:

$$B_l = \frac{S_l^i - S_l^v}{S_l^i}, \tag{29}$$

$$B_s = \frac{S_s^i - S_s^v}{S_s^i}, \tag{30}$$

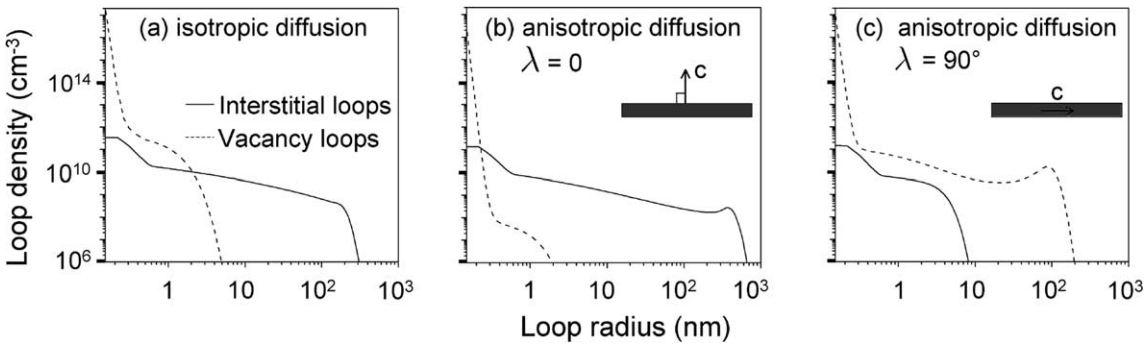

Fig. 5. Interstitial and vacancy loop size distributions in a Zr thin foil irradiated with electrons (1.5×10^{-4} dpa s^{-1}) up to 10 dpa: (a) SIA diffusion is supposed isotropic; (b,c) the SIA diffusion anisotropy is taken into account with two different foil orientations ($\lambda = 0$ and $\lambda = 90°$). λ is the angle between the normal to the foil surfaces and the c crystallographic axis.

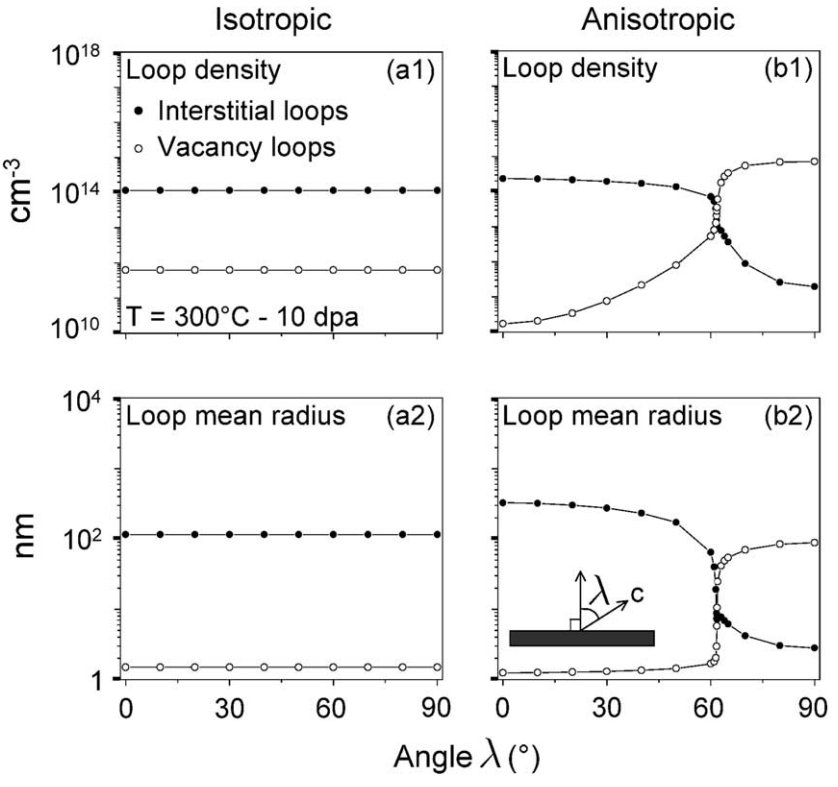

Fig. 6. Zr thin foil irradiated with electrons (1.5×10^{-4} dpa s^{-1}) up to 10 dpa. Effect of the foil crystallographic orientation on the loop density and the loop mean radius. Full symbols corresponds to interstitial loops and empty symbols correspond to vacancy loops. (a1, a2) SIA diffusion is supposed isotropic ($p = 1$). (b1, b2) SIA diffusion anisotropy is taken into account ($p = 0.775$).

where the S terms represents the sink strengths. The subscripts 'l' and 's' refer to the kind of sink (loops or surfaces) and the superscripts i and v refer to the nature of the point defects (SIA or vacancies). The sink strengths are defined as follows:

$$S_{\mathrm{l}}^{i} = \frac{1}{D_i} \sum_{n=2}^{\infty} \left(\beta_{ni}^{i} C_{ni} + \beta_{nv}^{i} C_{nv} \right), \tag{31}$$

$$S_{\mathrm{l}}^{v} = \frac{1}{D_v} \sum_{n=2}^{\infty} \left(\beta_{ni}^{v} C_{ni} + \beta_{nv}^{v} C_{nv} \right), \tag{32}$$

$$S_{\mathrm{s}}^{i} = \frac{K_{\mathrm{s}}^{i}}{D_i}, \tag{33}$$

$$S_{\mathrm{s}}^{v} = \frac{K_{\mathrm{s}}^{v}}{D_v}, \tag{34}$$

where K_{s}^{i} and K_{s}^{v} are defined by Eq. (7). The sink strength of the total prismatic loop population is the same for SIA and vacancy except that for SIA we have to consider the SIA-dislocation elastic interaction ($Z_{d\mathrm{iso}}^{i}$) and the SIA diffusion anisotropy (Z_a^i defined by Eq. (27)). We simply have:

$$S_{\mathrm{l}}^{i} = Z_{d\mathrm{iso}}^{i} Z_a^i S_{\mathrm{l}}^{v}. \tag{35}$$

It follows that:

$$B_{\mathrm{l}} = 1 - \frac{1}{Z_{d\mathrm{iso}}^{i} Z_a^i}. \tag{36}$$

Since the loop density is quite high, K_{s}^{i} and K_{s}^{v} can be calculated here by Eq. (10) with $S_m^{\theta} \approx S_{\mathrm{l}}^{\theta}$ (we neglect the absorption of point defects on dislocation lines). It follows that:

$$S_{\mathrm{s}}^{i} = \frac{\sqrt{S_{\mathrm{l}}^{i}}}{d'}, \tag{37}$$

$$S_{\mathrm{s}}^{v} = \frac{\sqrt{S_{\mathrm{l}}^{v}}}{d}. \tag{38}$$

We finally get:

$$B_{\mathrm{s}} = 1 - \frac{1}{\sqrt{Z_{d\mathrm{iso}}^{i} Z_a^i}} \frac{d'}{d}, \tag{39}$$

where the ratio d'/d is given by Eq. (28). When $B_{\mathrm{l}} > B_{\mathrm{s}}$, the loops absorb more SIA than vacancies (which also means that the surfaces absorb more vacancies than SIA). In that case, the dislocation loops that grow are interstitial in nature. On the contrary, if $B_{\mathrm{l}} < B_{\mathrm{s}}$, the

dislocation loops will absorb more vacancies and will be vacancy in nature. Let us examine first the situation where SIA diffusion is supposed isotropic. We have $d' = d$ and $Z^i_a = 1$. Then B_l and B_s reduce to:

$$B_l = 1 - \frac{1}{Z^i_{d\,\mathrm{iso}}} \approx 0.091, \tag{40}$$

$$B_s = 1 - \frac{1}{\sqrt{Z^i_{d\,\mathrm{iso}}}} \approx 0.046. \tag{41}$$

When SIA diffusion is isotropic, we always have $B_l > B_s$. The dislocation loops are then expected to be interstitial in nature, in agreement with the experimental observations concerning irradiation of isotropic metals.

Let us turn now to the case where diffusion is anisotropic. We still consider a temperature of 300 °C. At this temperature, $p = 0.775$ and $Z^i_a = 1.25$. B_l and B_s are plotted against λ in Fig. 7. When λ is small, $B_l > B_s$ and *interstitial* loops will grow. On the contrary, when λ is high, $B_l < B_s$ and *vacancy* loop are expected to grow, in agreement with the calculations of the cluster dynamics model presented in Fig. 6. The angle λ_0 for which $B_l = B_s$ is $\lambda_0 = 62.1°$ and corresponds exactly to the angle λ_0 observed on Fig. 6, where the situation changes from interstitial loop growth to vacancy loop growth.

All the calculations presented above were made at 300 °C. The results obtained by the cluster dynamics model at other temperatures between 200 and 500 °C are very similar to those presented here, characterized by interstitial loop growth when $\lambda < \lambda_0$ and vacancy loop growth when $\lambda > \lambda_0$. Between 200 and 500 °C, λ_0 is lying in the range 60–65°.

Looking at the experimental results concerning electron irradiation of zirconium in a high voltage microscope, it seems clear that an increase of the angle λ favors the vacancy loop nucleation and growth. We have summarized the results of Griffiths et al. [4] and Hellio et al. [3] in Table 2. Griffiths et al. observed in some cases a mixed population of both vacancy and interstitial loops. The approximative percentages of vacancy loops indicated in Table 2 were plotted against λ in Fig. 8, although all the results were not obtained at the same temperature. It is clear that the percentage of vacancy loops strongly increases above a certain angle λ_0. This angle λ_0 seems to be less than the theoretical value ($\lambda_0 \approx 60°$). Nevertheless, it should be mentioned that there is a quite high experimental uncertainty on the foil orientation (±15°). Moreover, the cluster dynamics model used here does not take the whole complexity of the problem into account: in particular, the formation of an oxide layer on the foil during irradiation is often observed; this can induces some stresses in the foil and influence the nucleation and the growth of dislocation loops [6]. We can at least conclude that the results of the cluster dynamics model presented in Fig. 6 are in qualitative agreement with the experimental results deal-

Table 2
Experimental results of electron irradiation of a Zr thin foil in a high voltage microscope

	T (°C)	$\vec{n}$	λ	% of vacancy loops	Refs.
1	400–600	$[1\bar{1}04]$	30	0	[3]
2	312	$[1\bar{2}13]$	43	0	[4]
3	457	$[0\bar{2}23]$	45	≈70	[4]
4	402	$[1\bar{2}11]$	68	≈75	[4]

$\vec{n}$ is the direction of the normal to the foil surfaces. λ is the angle between $\vec{n}$ and the c-axis.

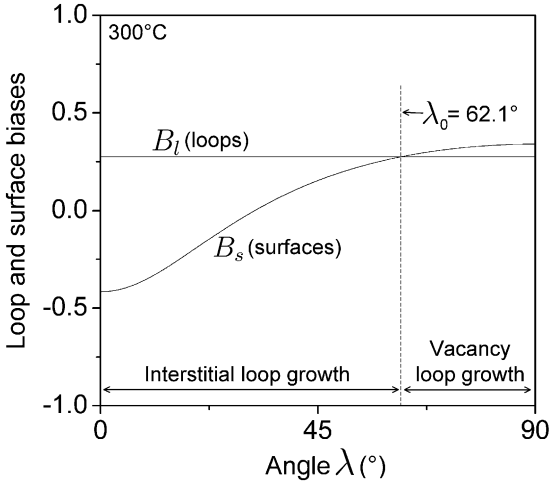

Fig. 7. Loop and surface biases B_l and B_s plotted against λ. $T = 300$ °C, $p = 0.775$, $Z^i_a = 1.25$ and $Z^i_{d\,\mathrm{iso}} = 1.1$.

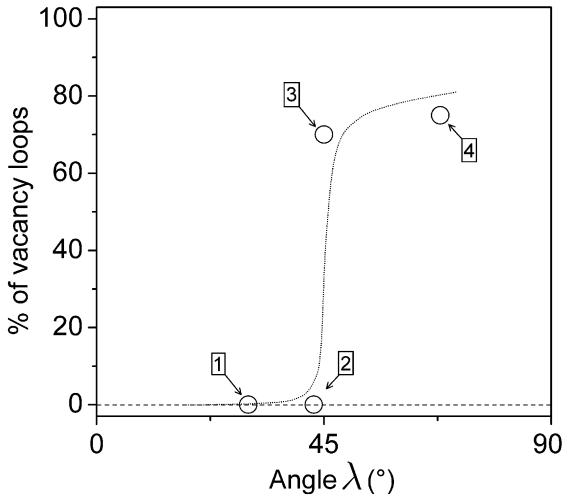

Fig. 8. Experimental results taken from Table 2 showing the influence of the foil orientation on the percentage of vacancy loops in electron-irradiated Zr. The numbers indicated on the figure correspond to the numbers in Table 2.

ing with the influence of the foil orientation on the dislocation loop microstructure under electron irradiation of zirconium.

5. Conclusion

Following the approach proposed by Woo [2], the cluster dynamics model presented in [1] that describes point defect agglomeration under irradiation was extended to the case where SIA diffusion is anisotropic. This new model was then applied to describe the evolution of the dislocation loop microstructure in zirconium under electron irradiation in a high voltage microscope (only the prismatic loops were considered here). The inputs of the model were first validated by comparing the results of the model to the experimental results of Hellio et al. [3]. The only fitting parameter was the di-interstitial binding energy E_{2i}^{B}. We found $E_{2i}^{B} = 1.42$ eV, in good agreement with the value obtained by de Diego et al. using molecular dynamics simulations [16].

Calculations made with different foil orientations show that the foil orientation has a very sensitive effect on the loop microstructure. This effect is directly linked to the SIA diffusion anisotropy. When the *c* crystallographic axis is normal to the foil, *interstitial* loops grow, whereas when the *c* crystallographic axis is parallel to the foil, *vacancy* loops grow. This can be interpreted by comparing the bias of surfaces and prismatic dislocation loops. The numerical results are in qualitative agreement with experimental results [3,4], which means that SIA diffusion anisotropy provides a reliable explanation to the 'unexpected' observation of vacancy loops in zirconium irradiated with electrons in a high voltage microscope.

References

[1] A. Hardouin Duparc, C. Moingeon, N. Smetniansky-de-Grande, A. Barbu, J. Nucl. Mater. 302 (2002) 143.
[2] C.H. Woo, J. Nucl. Mater. 159 (1988) 237.
[3] C. Hellio, C.H. de Novion, L. Boulanger, J. Nucl. Mater. 159 (1988) 368.
[4] M. Griffiths, M.H. Loretto, R.E. Sallmann, J. Nucl. Mater. 115 (1983) 313.
[5] M. Griffiths, M.H. Loretto, R.E. Sallmann, J. Nucl. Mater. 115 (1983) 323.
[6] M. Griffiths, M.H. Loretto, R.E. Sallmann, Philos. Mag. A 49 (1984) 613.
[7] J. Nucl. Mater. 159 (1988) 237. Proceedings of the International Conference on Fundamentals Mechanisms of Radiation Creep and Growth, Hecla Island, Manibota, Canada, 22–25 June 1987.
[8] M. Griffiths, J. Nucl. Mater. 159 (1988) 190.
[9] W. Franck, J. Nucl. Mater. 159 (1988) 122.
[10] D.J. Bacon, J. Nucl. Mater. 159 (1988) 176.
[11] Y.N. Osetsky, D.J. Bacon, N. de Diego, Metall. Mater. Trans. A 33A (2002) 777.
[12] R. Bullough, M.R. Hayns, M.H. Wood, J. Nucl. Mater. 90 (1980) 44.
[13] N. Soneda, T. Diaz de la Rubia, Philos. Mag. 78 (1998) 995.
[14] L.K. Mansur, Philos. Mag. A39 (1979) 497.
[15] R.A. Holt, R.W. Gilbert, J. Nucl. Mater. 137 (1986) 185.
[16] N. de Diego, Y.N. Osetsky, D.J. Bacon, Metall. Mater. Trans. A 33A (2002) 783.
[17] G.J. Ackland, S.J. Wooding, D.J. Bacon, Philos. Mag. A 71 (1995) 553.
[18] R.C. Pasianot, A.M. Monti, J. Nucl. Mater. 264 (1999) 198.
[19] S.R. MacEwen, R.H. Zee, R.C. Birtcher, C. Abromeit, J. Nucl. Mater. 123 (1984) 1036.
[20] P. Ehrhart, B. Schönfeld, in: J.I. Takamura, M. Doyama, M. Kiritani (Eds.), Point Defects and Defect Interactions in Metals, North Holland, Amsterdam, 1982, p. 47.